3D WAVE PROPAGATION AND SITE EFFECTS IN THE HUMBOLDT BAY AREA USING STRONG GROUND MOTION RECORDS FROM THE M6.5 2010 FERNDALE EARTHQUAKE.

Arben Pitarka[1], Hong Kie Thio[2] and Paul Somerville[2]

[1]Lawrence Livermore National Laboratory, Livermore
[2]URS Corporation, Los Angeles

Abstract

In this study we simulated and analyzed strong ground motion data recorded in the Humboldt Bay and Eureka areas during the M6.5 Ferndale area earthquake of January 2010. The scope of the presented work was two-fold. First, we investigated the main aspects of seismic wave generation and propagation, including kinematic rupture process and 3D wave propagation scattering. Our goal is to analyze their potential effects on seismic motion recorded at free field stations across Humboldt Bay and Eureka, and test the performance of a standard broadband strong ground motion simulation technique. Second, using non-linear site response analysis, we investigated the effects of shallow sedimentary layers on strong ground motion recorded by the Humboldt Bay geotechnical array. Our study provides insight into the composition of the wave field during the earthquake and an improved understanding of how the wave field is affected by the local 3D structure and the non-linear response of the shallow sediments of the Humboldt Bay.

Introduction

The M6.5 Ferndale earthquake occurred north of the Mendocino Triple junction, in a region with complex structure caused by subducting plates. This strike-slip earthquake occurred at a depth of about 29 km within the subducting Gorda plate, with a preliminary estimate of the depth extent of faulting ranging between about 10 and 20 km (U.C. Berkeley). Damage was concentrated along the coast from Ferndale to Eureka. Areas founded on deep estuary and river deposits had higher damage compared with areas located on shallower soils and rock (Storesund, 2010). In Figure 1, we compare the recorded ground motions with the ground motions predicted by the NGA ground motion prediction equations for crustal earthquakes (Abrahamson et al., 2008) and the ground motion model for intraslab earthquakes of Zhao et al. (2006). The NGA ground motion prediction equations have more gradual attenuation with distance than the recorded ground motions, and do not provide a good fit to their amplitudes. This is not surprising, because the earthquake was clearly a mantle earthquake, not a shallow crustal earthquake of the kind modeled by the NGA ground motion prediction equation used here. Its location below the oceanic Moho in a region that is expected to have a low velocity gradient apparently resulted in rapid attenuation, because there is no strong velocity gradient such as the Moho to cause the gradual attenuation of ground motions from crustal earthquakes (e.g. Somerville *et al.,*1984). In general the peak amplitude of ground motion acceleration recorded

along the coast (distances between 40km and 55km) is much higher than predicted by both ground motion prediction equations. The largest recorded ground acceleration and velocity were about 44% g and 47 cm/s respectively at Ferndale, about 43 km east of the epicenter.

The Zhao et al. (2006) model is derived from normal and thrust faulting mantle earthquakes at depth within subducted slabs, whereas the 2010 Ferndale earthquake was a strike-slip earthquake that occurred within the shallow part of the slab that lies oceanward of the subduction zone. It nevertheless provides a better fit to the recorded ground motions, having a rate of attenuation similar to that of the data.

The complexity of the source process, and the three-dimensional underground structure need to be considered when analyzing the strong ground motions recorded during the earthquake. Their potential contributions to the double pulse-like motion and large variability of peak acceleration recorded at stations with similar source distance is the focus of our investigation.

Strong Motion Records

In our investigation we used ground motion data recorded by over 20 free-field strong-motion stations of the California Geological Survey (CGS) and U.S. Geological Survey, and the vertical geotechnical array, posted at the Center of Engineering Strong Motion Data web site. The corrected three component accelerograms were downloaded from the website of the CGS strong motion center (http://www.strongmotioncenter.org). This data set provides an excellent resource to analyze wave propagation and local site effects.

The location of the strong motion sites, and the location of four selected sites that were used in our preliminary data analysis, are shown in Figure 2. A photo of the bridges in the Humboldt Bay area, where the geotechnical array is located, is shown in Figure 3.

Three-Dimensional Velocity Model

We used geotechnical data for the area (e.g. Clarke, 1992) and available geophysical and geological profiles to extend the 3D velocity model of the Eel River basin developed by the URS group (Graves, 1994). The URS velocity model was originally developed to the study ground motion and rupture process of the 1992 Cape Mendocino earthquake (Graves, 1994). Our model extended to the north and includes the Humboldt Bay and Eureka areas. The map of the basin depth is shown in Figure 4. The offshore basin structure is not well resolved by the available data. Therefore we assumed a rather flat geometry that extends east of the fault. The background crustal model is based on GIL7, a 1D regional velocity model (Dreger, 2011, personal communication). In our model, the basin sediments are represented by two layers with a minimum velocity of 620 m/s. In our long period ground motion simulation we used a 200 m grid spacing which allow for accurate finite-difference computation of the wave field up to 0.8 Hz. A map view and a vertical cross-section of the 3D velocity model are shown in Figure 5.
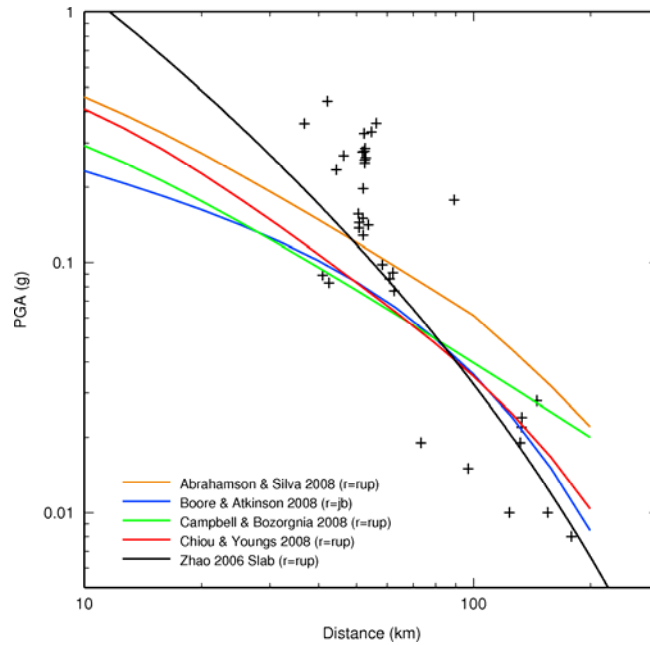
Figure 1. Comparison of recorded peak acceleration of the 2010 Ferndale earthquake with the predictions of the NGA (Abrahamson et al., 2008) ground motion models for shallow crustal earthquakes and the Zhao et al. (2006) ground motion prediction model for intraslab earthquakes
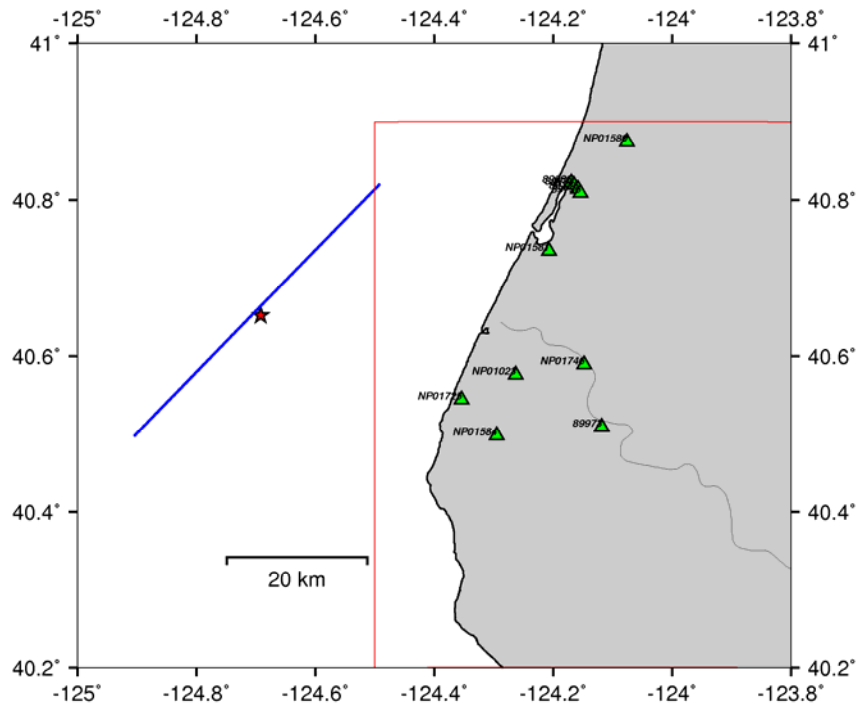
Figure 2. Map of the study area showing the stations location (triangles), ocean-bottom fault projection (blue line), and epicenter location (star). Red square indicates the area for which a 3D model for the shallow sediments was developed.

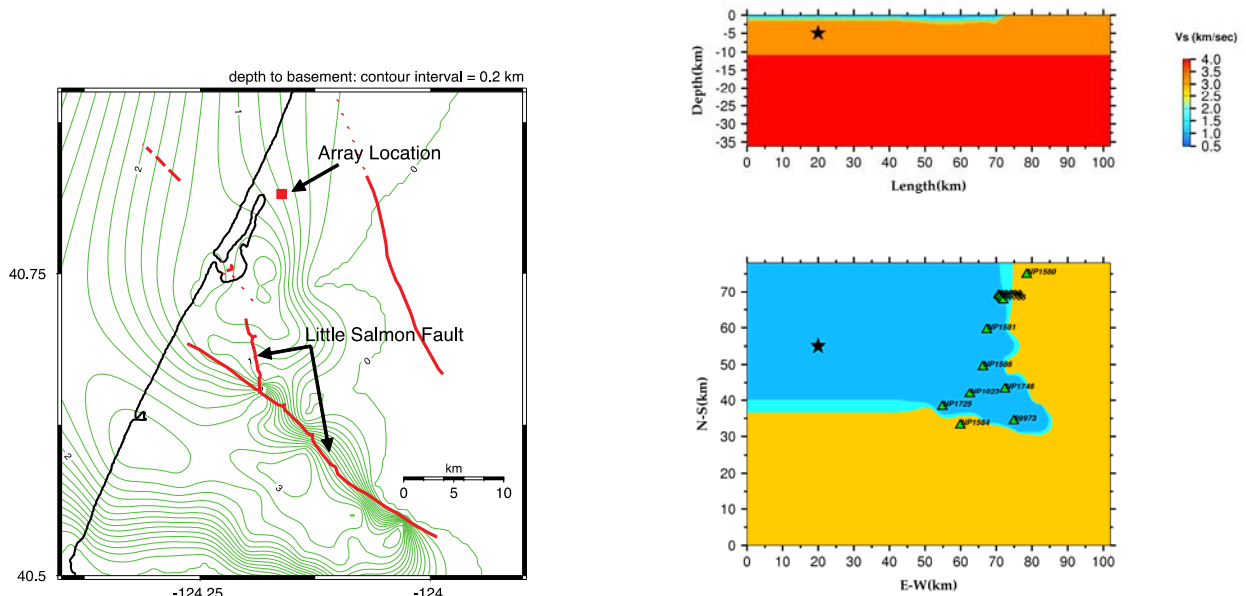**Figure 3**. Humboldt Bay Middle Channel Bridge (courtesy of Caltrans)

Figure 4. Left panel: Map of the basin depth. Green contour lines show depth to the basement, and red lines indicate location of major faults. The array location is shown by the red square. Right panel: The three-dimensional velocity model. Top Panel: E-W vertical section crossing the epicenter. Bottom Panel: Map view of the basin showing the strong motion stations location (triangles), and earthquake epicenter (star).

Broad-Band Strong Ground Motion Modeling

Kinematic Slip Model

Analysis of the earthquake indicates that slip occurred on a near-vertical, left-lateral fault oriented about N47E. Large strike-slip earthquakes like this one are common in the interior of the Gorda plate. The hypocenter was located at a depth of 29 km, but accuracy is relatively poor owing to the earthquake occurring about 40 km offshore and 56 km from the nearest seismic station. Preliminary inversion of long period ground motion displacement by the UC Berkeley Seismological Laboratory (Dreger, 2010, personal communication) estimated a fault length of about 25 km; rupture proceeded unilaterally to the southwest. The peak estimated slip between the two sides of the fault was 2.4 meters.

We started the investigation of the source process by simulating ground motion velocity at 11 stations located along the coast. Our simulation using 3D Green's functions (Pitarka, 1999) indicates that the original kinematic slip model does a poor job at explaining the recorded data. Based on trial and error analysis we produced a refined kinematic rupture model that explains the overall characteristics of recorded strong ground motion in a broad frequency range. The slip model is shown in Figure 5. The fault geometry is the same and the mechanism is similar to UC Berkeley's model. We use a strike angle of 230 degrees, dip angle of 86 degrees, rake angle of 11 degrees, maximum rupture velocity of 2.8 km/s, and a maximum rise time of 1.7s. The local slip is represented by two time-windows with a 0.3 s overlapping. The subfault dimensions are 1 by 1km. The details of the rupture kinematics are not well resolved due to poor station distribution and limited knowledge of underground structure in the source region. Our kinematic model suggests that the rupture was bilateral, and a zone of large slip was located north of hypocenter, with a maximum slip of 1.2 m.
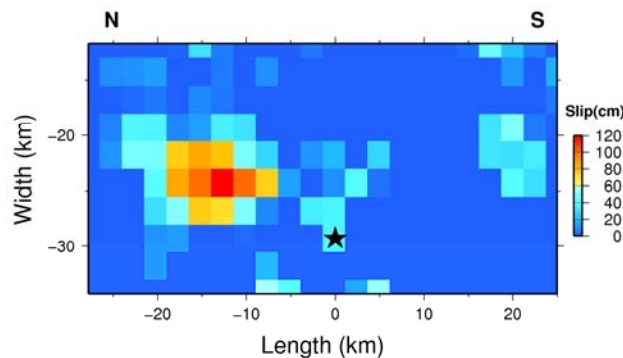
Ground Motion

We used the broad-band simulation procedure of Graves and Pitarka (2010) to simulate strong ground motion at 11 stations shown in Figure 2. The broadband ground-motion simulation procedure is a hybrid technique that computes the low-frequency and high-frequency ranges separately and then combines the two to produce a single time history. At frequencies below 1 Hz, the methodology is deterministic and contains a theoretically rigorous representation of fault rupture and wave propagation effects, and attempts to reproduce recorded ground-motion waveforms and amplitudes. At frequencies above 1 Hz, it uses a stochastic representation of source radiation, which is combined with a simplified theoretical representation of wave propagation and scattering effects. The simulation uses site corrections proposed by Campbell and Bozorgnia (2008) using Vs30.

The comparison between recorded and simulated time histories and response spectra of acceleration, and velocity at 11 sites located along the coast is shown in Figure 6 and Figure 7, respectively. Due to primarily bilateral rupture initiating at the center of the fault, the Ferndale event produced strong rupture directivity effects toward the northeast and southwest. Due to their relative location with respect to the fault most of the sites are affected by the rupture

directivity toward the north. The large velocity pulse observed on the N-S component at stations north-east of epicenter is well reproduced by the simulation. This pulse is controlled by the rupture directivity to the north. T he large pulse observed on the E-W component at sites south-east of epicenter is not well reproduced by the simulation. This could indicate that the second asperity located south of the rupture initiation has a much larger slip.

We compute the model bias and standard error for 5% damped spectral acceleration over a suite of periods from 0.05 to 8 s for the simulation using 11 sites. The results are displayed in Figure 7 for the fault-parallel, fault-normal, and average horizontal (geometric mean) components. The model bias is near zero for all components across the entire bandwidth indicating that, on average, the simulation is accurately reproducing the main characteristics of the observed ground motions. The largest standard error for these comparisons is about 0.2 natural log units for periods less than about 0.8 s. For periods longer than 0.8 s, the standard error increases to about 0.4 natural log units. The increased standard error at the longer periods is probably due to deficiencies in our assumed rupture model, which have a relatively stronger impact on the deterministic aspects of the simulation.


Figure 5. Kinematic slip model developed in this study

Nonlinear Soil Response Analysis

The ground motions from the 2010 Ferndale earthquake recorded at the Humboldt Bay geotechnical array provide another opportunity for testing the efficiency of current nonlinear techniques for predicting soil response under moderate shaking. The array is located about 0.25 mile north-west of the west abutment of the Middle Channel Bridge (see Figure 3). It contains four borehole instruments installed at the free surface and at depths of 19m, 33m, 56m, and 136m. The corrected three component accelerograms were downloaded from the website of the CGS strong motion center (http://www.strongmotioncenter.org).

We used the computer program NOAH_SH based on the nonlinear soil response technique of Bonilla et al. (2005) to analyze the recorded response at borehole instruments. NOAH_SH is based on the staggered-grid finite-difference method and Iwan's (1967) nonlinear soil model.
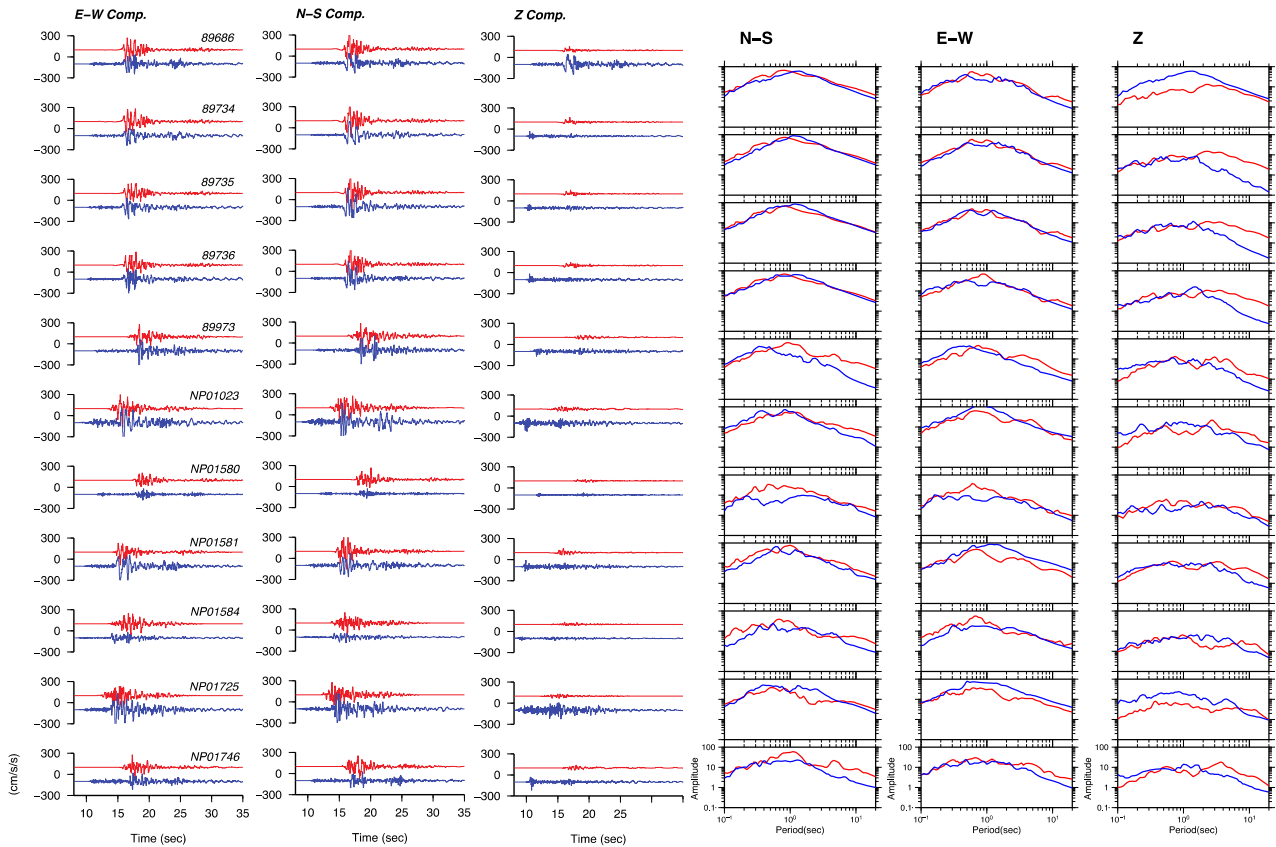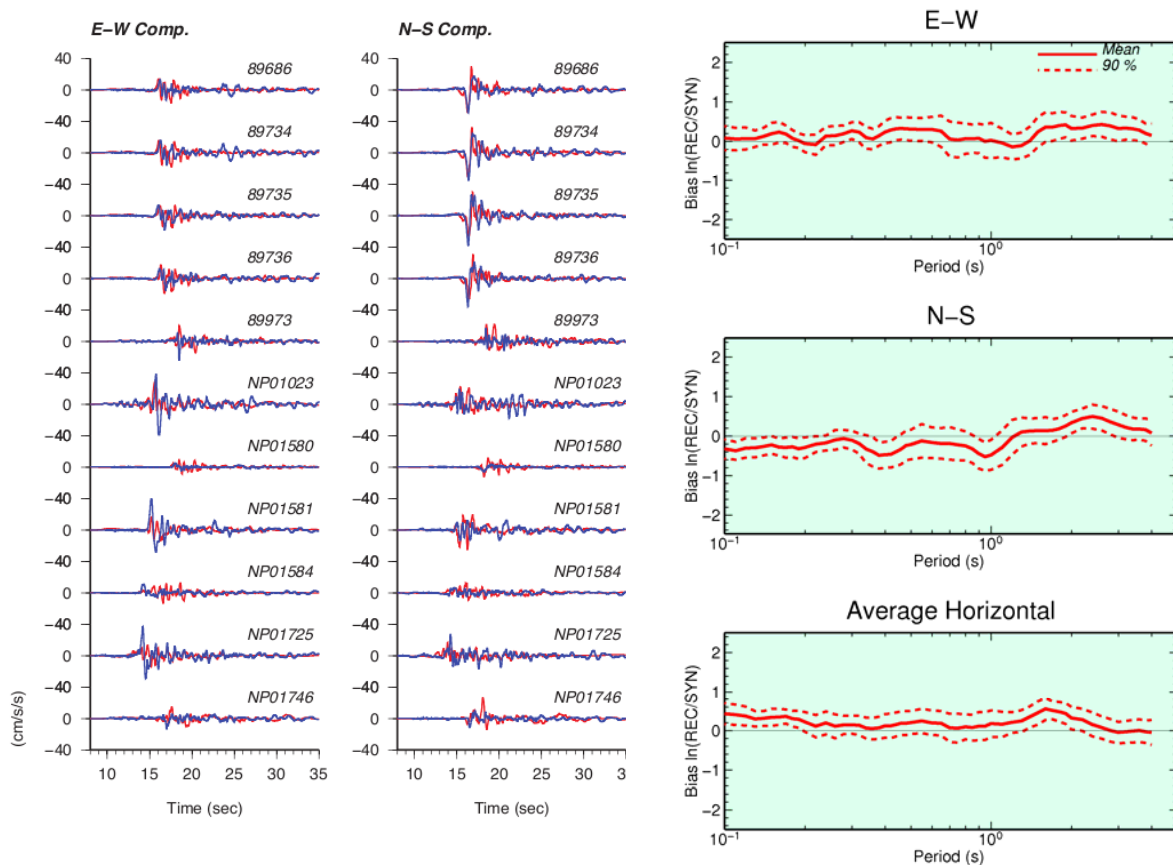
Figure 6. Comparison of simulated (red traces) and recorded (blue traces) ground motion acceleration. Left panel: acceleration time histories. Right panel: acceleration response spectra.

The technique operates in the time domain by tracking the earthquake load through stress-strain space. It allows the direct use of G/Gmax laboratory data that can be assigned to each layer. Typically it uses the Masing rule for unloading and re-loading that may result in an over-prediction of hysteretic damping at large strains. Reviews of the methodology can be found in the work of Joyner and Chen (1975) and Bardet (2001). Recent applications of the NOAH_SH computer program as well as comparisons with other traditional methods such as the equivalent linear method are shown in the study of Hartzell *et al.* (2004). Our choice of a fully nonlinear technique is based on the fact that nonlinear finite-difference techniques have several advantages over the classical equivalent nonlinear method. First, with a finite difference method one can easily obtain the strain from the node displacement gradient that is then introduced into the constitutive equation to compute the stress. Second, the constant damping, independent of frequency, used in the equivalent nonlinear methods causes the over-attenuation of high frequencies. This unrealistic feature becomes more pronounced at high levels of strain.

In our site response analysis we used the Peninsular Range (PR) modulus reduction, *G/G*max, and damping curves as a function of shear strain for cohesionless soil developed by Silva et al. (1997, 1999) and the Vucetic and Dobry (1991) curves for a plasticity index of 30 for the top clay layers. The PR curves are a subset of the EPRI (1993) curves developed by modeling recorded motion. We used them for soils below 7 m.

The 1D velocity model used in the non-linear simulations is based on borehole shear-wave speeds provided by Caltrans. The shear wave velocity increases from about 180 m/sec at the free surface to 630 m/s in hard rock at 220 m depth. The shear wave velocity profile is shown in Figure 8.

Figure 9 compares time histories and amplitude spectra of recorded and computed acceleration at the geotechnical array. The recorded E-W component of the acceleration at a depth of 136 m was used as input motion to compute the non-linear response of the shallow sedimentary layers. The synthetic accelerograms compare well with the recorded accelerograms at all depths. Similarly Figure 10 compares the recorded and simulated time histories of acceleration assuming a linear soil response. The simulation results clearly shows that in comparison with linear response the non-linear response of soils suppresses much of the high frequency energy as the waves propagate through the soil column. Significant non-linear response is observed even at a depth of 56 m.

Figure 7. Left panel: Comparison of simulated (red) and recorded (blue) ground motion velocity time histories. Right panels: Model bias (heavy line) and standard error (shaded between dotted lines) for 5% damped spectral acceleration using 11 sites. Top panel shows the fault-parallel component, middle panel shows the fault-normal component and bottom panel shows the average horizontal (geometric mean) component.
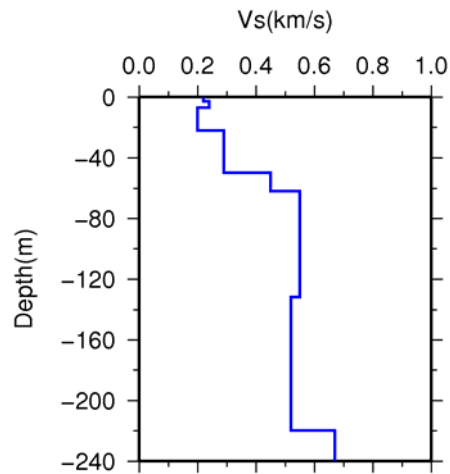
Figure 8. Shear-wave velocity profile used in the 1D non-linear analysis

Conclusion

In order to reproduce the recorded peak amplitude of ground motion, the stress drop used in our broad-band simulations is about 25% higher than the one we use in typical simulations of strike-slip faults for crustal earthquakes. This indicates that the stress drop of the Ferndale earthquake was relatively high. Our finding is in agreement with observations made for deep earthquakes of similar type.

Our wave propagation modeling demonstrates that the fault rupture was bilateral, and that rupture directivity was strong on both rupture directions. Basin induced waves caused a second large pulse, and amplified ground motion at basin sites. This is illustrated in Figure 11 which compares recorded acceleration decomposed into empirical modes (Huang et al., 1998) at two free-field basin sites (NP01581, geotechnical array 89734) and site NP01580, located outside the basin. The second large pulse is strong at all sites inside the basin. In contrast, such pulse is not observed at rock sites. Based on analysis of simulated ground motion using 3D models with and without the basin structure we concluded that the second large pulse observed at basin sites is a basin induced wave. The basin and local site effects contributed to large amplification of ground motion at soils sites along the coast.

1D wave propagation analysis at the geotechnical array, using a fully non-linear numerical technique, show that the seismic response of soft sedimentary layers in the Humboldt Bay can be well modeled by a fully non-linear technique. The next step in our study will be the investigation of the sensitivity of the computed waveforms to velocity variation in the approximate 1D velocity models used in the non-linear soil response analysis. The effect of input motion characteristics on the non-linear response at the geotechnical array will be finally investigated by using broad-band synthetic accelerograms from the 2010 Ferndale earthquake, simulated during this study.
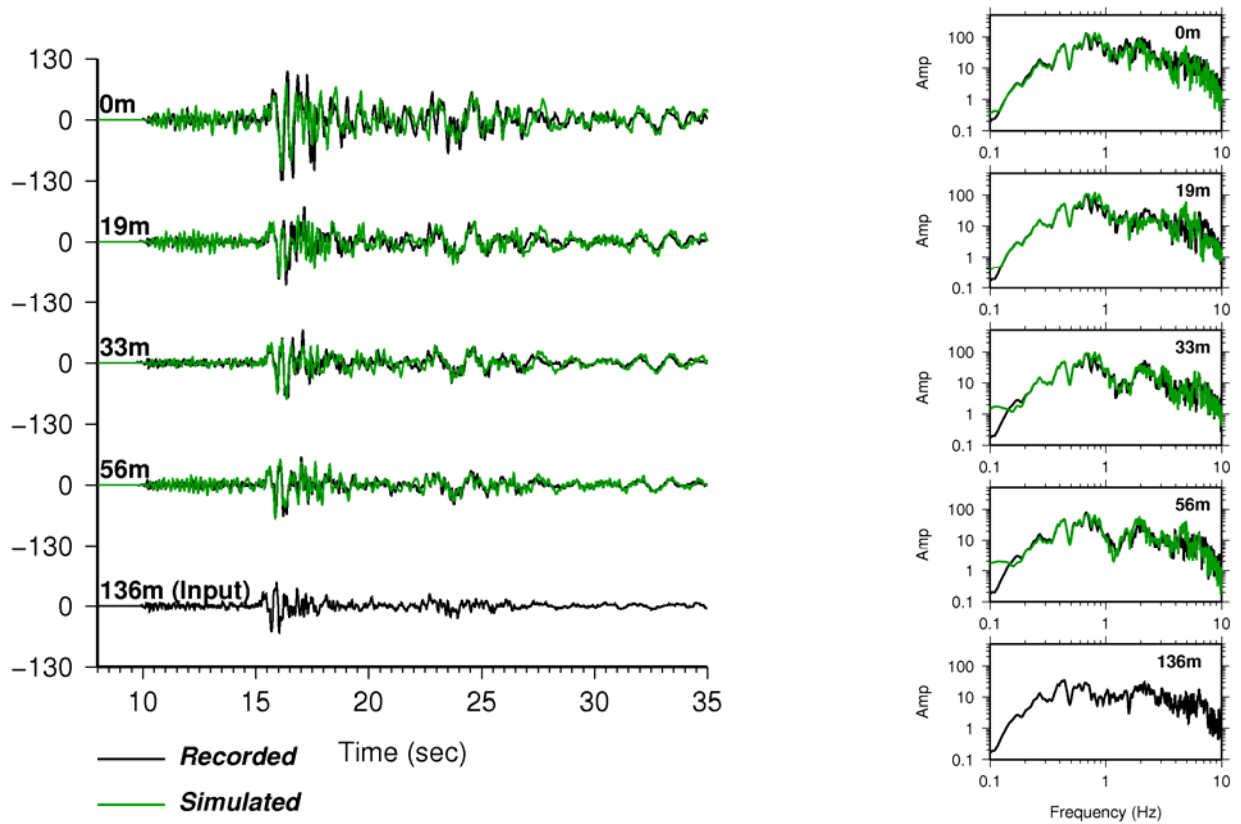
Figure 9. Comparison between recorded (black traces) and synthetic (green traces) acceleration calculated at borehole stations using the non-linear technique. The input motion is applied at a depth of 136 m.
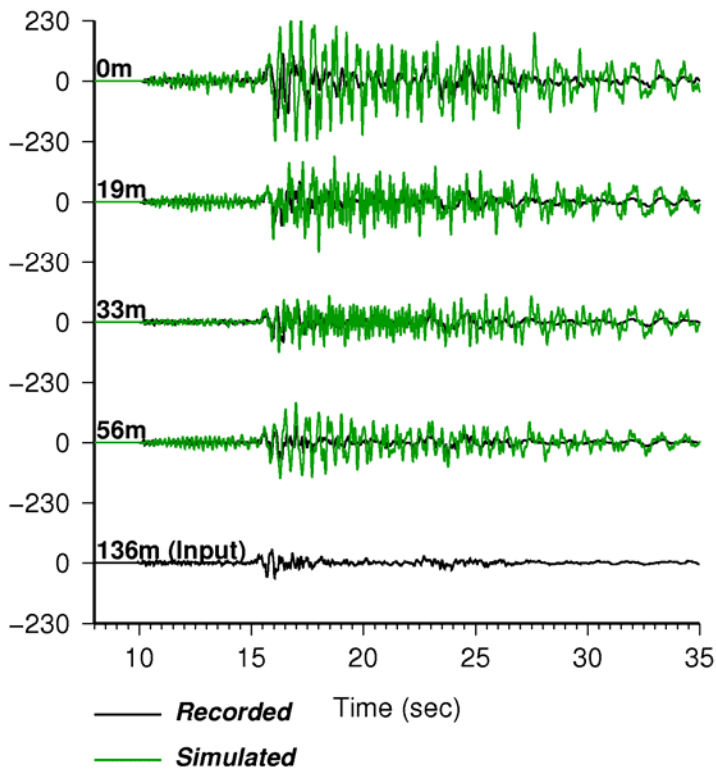
Figure 10. Comparison between recorded (black traces) and synthetic (green traces) acceleration calculated at borehole stations using linear response of soils.
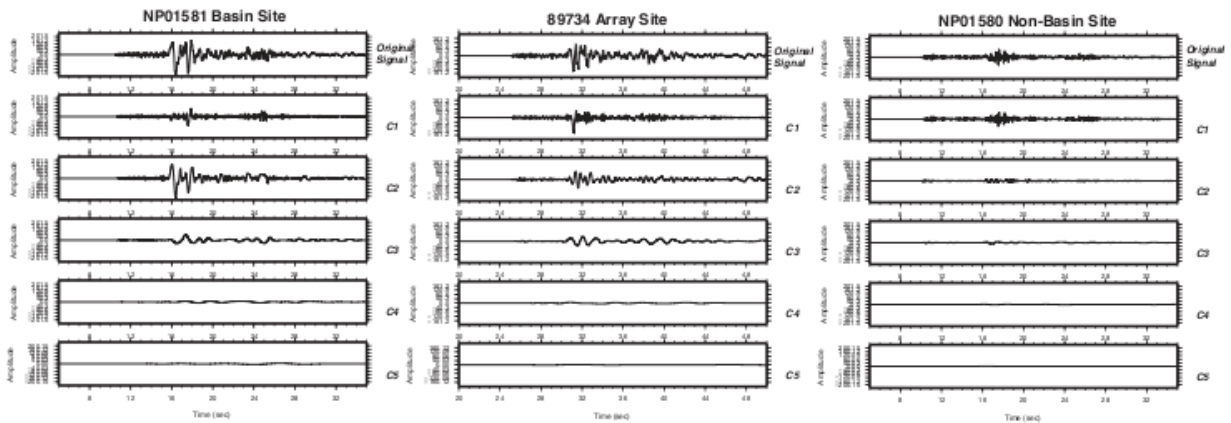
Figure 11. Empirical mode decomposition (Ci) of the horizontal acceleration recorded at free-field stations NP01581, geotechnical array 89734, and NP01580. The second large pulse that dominates the second mode. This pulse of relatively low frequency is only visible in basin sites.

References

Abrahamson, N.A., G.M. Atkinson, D.M. Boore, Y. Bozorgnia, K.C. Campbell, B. Chiou, I. M. Idriss, W.J. Silva, and R.R. Youngs (2008). Comparisons of the NGA Ground-Motion Relations. Earthquake Spectra 24, 45-66.

Bardet, J.P. and T. Tobita (2001). NERA a computer program for Nonlinear Earthquake site Response Analyses of Layered Soil Deposits, Department of Civil Engineering, University of Southern California, 46 pp.

Bonilla, L. F. (2000). Computation of linear and nonlinear site response for near field ground motion, *Ph.D. Thesis*, University of California, Santa Barbara.

Bonilla, L., F., R. Archuleta, and D. Lavallee (2005). Hysteretic and dilatant behavior of cohesionless soils and their effects on nonlinear site response: field data, observations and modeling, Bull. Seism. Soc. Am., 95, 2373-2395.

Clarke, S. H. (1992). Geology of the Eel River basin and adjacent region: Implications for late Cenozoic tectonics of the southern Cascadia Subduction Zone and Mendocino Triple Junction, AAPG Bulletin, 76, 199-224.

Graves R. W. (1994). Rupture history and strong ground motion modeling of the 1992 Cape Mendocino earthquake. Report to USGS, award # 1434-93-G-0237.

Graves, R. W. and A. Pitarka (2010). Broadband ground-motion simulation using a hybrid approach. Bull. Seism. Soc. Am., 100, 5A, 2095-2123.

Hartzell, S.H., L.F. Bonilla, and R.A. Williams (2004). Prediction of nonlinear soil effects, Bull. Seism. Soc. Am., 94, 1609-1629.

Huang, N. E., Shen, Z., Long, S. R., Wu, M. C., Shih, E. H., Zheng, Q., Tung, C. C. & Liu, H. H. (1998). The empirical mode decomposition method and the Hilbert spectrum for non-stationary time series analysis. *Proc. R. Soc. Lond.* A**454**, 903–995.

Iwan, W.D. (1967). On a class of models for the yielding behavior of continuous and composite systems, J. of App. Mech., 34, 612-617.

Joyner, W., and A.T. Chen (1975). Calculation of nonlinear ground response in earthquakes, Bull. Seism. Soc. Am., 65, 1315-1336.

Pitarka, A. (1999). 3D elastic finite-difference modeling of seismic motion using staggered grids with nonuniform spacing. *Bull. Seism. Soc. Am*. 89, 54-68.

Silva, W., N. Abrahamson, G. Toro, and C. Costantino (1997). Description and validation of the stochastic ground motion model, Report submitted to Brookhaven National Laboratory, Associated Universities, Inc., Upton, New York 11973, Contract No. 770573.

Silva, W., Li, S., B. Darragh, and N. Gregor (1999). Surface geology based strong motion amplification factors for the San Francisco Bay and Los Angeles areas. Pearl Report to PG&E/CEC/Caltrans. (http://www.pacificengineering.org).

Somerville, P.G., N.F. Smith, and R.W. Graves (1994). The effect of critical Moho reflections on the attenuation of strong motion from the 1989 Loma Prieta earthquake, in "The Loma Prieta, California, Earthquake of October 17, 1989 - Strong Ground Motion," U.S. Geological Survey Professional Paper 1551-A, A67-A75.

Storesund, R., L. Dengler, S. Mahin, B.D. Collins, M. Hanshaw, F. Turner, K. Welsh (2010). M6.5 Earthquake Offshore Northern California January 9, 2010. GEER Field Reconnaissance Summary.

Vucetic, M., and R. Dobry (1991). Effect of soil plasticity on cyclic response, J. Geotech. Eng. ASCE 117, 89–107.

Zhao J.X., Zhang J., Asano A., Ohno Y., Oouchi T., Takahashi T., Ogawa H., Irikura K., Thio, H.K., Somerville P.G., Fukushima Y. (2006). Attenuation relations of strong ground motion in Japan using site classification based on predominant period. *Bull. Seism. Soc. Am*. 96, 914–925.